CHINESE OPTICS LETTERS

Vol. 21, No. 9 | September 2023

Babinet's meta-apertures for holographic bi-imaging

Syed Yasir Azeem, Dong Zhao (赵 东), Ruixing Xia (夏睿星), and Kun Huang (黄 坤)*

Department of Optics and Optical Engineering, University of Science and Technology of China, Hefei 230026, China

*Corresponding author: huangk17@ustc.edu.cn

Received May 24, 2023 | Accepted June 19, 2023 | Posted Online August 14, 2023

Complementary metasurfaces based on Babinet's principle have shown remarkable performance in optical applications like polarization conversion and split ring resonators by dynamically reversing the properties of light in both transmission and reflection modes. However, complementary diffractive metasurfaces for different holographic images have not yet proven to be effective because Babinet's principle predicts identical diffraction patterns from complementary surfaces. Here, we report carefully designed complementary metasurfaces consisting of an engineered metallic aluminum layer sitting on a transparent quartz substrate. Upon illumination, both complementary devices output entirely different diffractive intensity profiles from each other, yielding two holographic images at visible wavelengths from 430 nm to 650 nm. It provides experimental evidence for encoding two images into complementary metasurfaces, indicating an exception of Babinet's principle in the Fresnel region of complementary apertures.

Keywords: Babinet's principle; metasurfaces; holography.

DOI: 10.3788/COL202321.090501

1. Introduction

Metasurfaces[1] are gaining momentum in scientific research for the advantages in controlling properties of light such as phase[2], intensity[3], and polarization[4]. These properties have recently extended the scope of metasurfaces for use in holography. Metasurfaces are widely used[5,6] in designing holograms that offer various degrees of freedom or methods for multiplexing[7] these options into a single device. Various optical principles are employed to design metasurfaces specifically for holographic applications[8]. An important principle governing diffractive optics is Babinet's principle, which states that the diffraction pattern produced by an opaque object is equal to the diffraction pattern produced by a complementary aperture (a hole of the same size and shape) placed in an opaque screen. This principle is utilized in the design of optical filters and antennas to produce similar diffraction patterns without the need for complex geometries or additional components[9].

Babinet's principle has been used in designing metasurfaces previously that had complementary split ring resonators[10] for high-frequency selectivity and negative dielectric permittivity. Using Babinet's principle, Luo *et al.* also designed a novel metasurface exhibiting strong circular dichroism (CD) and dynamic reversibility. They demonstrated that the metasurface is designed to be Babinet-invertible, i.e., it has the same optical response when its electric and magnetic properties are swapped[11]. Similarly, an anisotropic Babinet-invertible metasurface design was proposed[12] and realized for achieving transmission–reflection switching for orthogonal polarizations of light. The design uses Babinet's principle to create a complementary structure that exhibits opposite polarization-dependent properties compared to the original metasurface. The proposed design demonstrates the potential of Babinet-invertible metasurfaces in achieving polarization-dependent optical functionalities.

Babinet's principle has been used to predict and optimize different metasurfaces for manipulating and predicting the outcome of metasurfaces according to the desired properties. The applications of complementary diffractive surfaces to optimize holograms have not yet been possible in holography due to the limitations in producing hologram patterns caused by identical diffraction from complementary surfaces. It is extremely important to find alternative ideas for multiple degrees of freedom in metasurface holography, as the recent research in the modulation of light through diffractive surfaces is at its peak and could potentially be vital to holographic and imaging applications in the future. In this work, we propose a device carefully designed and optimized to employ two different holograms potentially having applications simultaneously in transmission and reflection modes. Two complementary diffractive surfaces will be designed to produce different holographic patterns after the light is transmitted through the diffractive surfaces.

2. Methods and Materials

2.1. Methods

Figure 1(a) shows a schematic of the proposed mask with a beam of light incident on its surface, where it produces a pattern of an

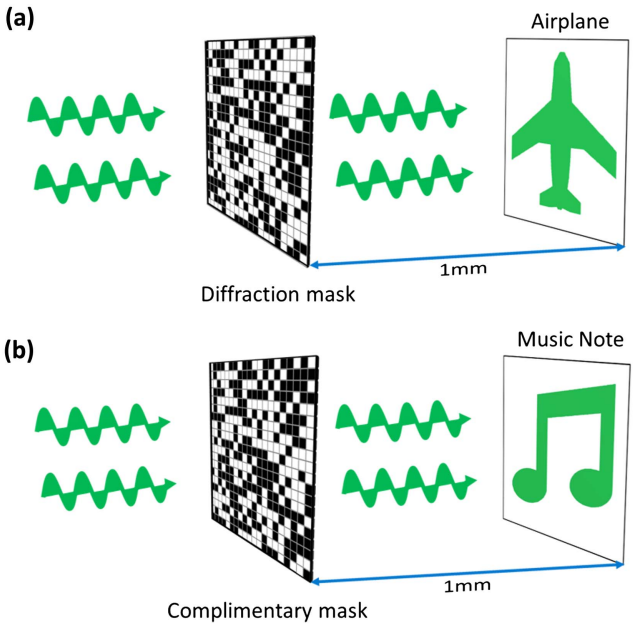

Fig. 1. Schematic of the proposed light modulating device inspired by Babinet's principle's complementary parts of the diffractive surface. (a) An optimized mask is meant to produce a pattern of one of the holograms (airplane in this case). (b) The complementary one is to produce another holographic pattern (such as the music note here). Each pixel has the pitch of 250 nm × 250 nm.

'airplane' after passing through the mask, while its complementary device, as illustrated in Fig. 1(b), can also produce another hologram pattern of a 'music note.' If one mask has the binary-amplitude modulation of $A(x_0, y_0)$ (where x_0 and y_0 are the spatial coordinates at the mask plane), one can obtain the modulation $B(x_0, y_0) = 1 - A(x_0, y_0)$ for its complementary mask. Mathematically, we describe the diffraction of light from both complementary masks by using

$$U_a(x, y, z) = \iint_{\Sigma} A_0(x_0, y_0) \frac{\partial}{\partial z}\left(\frac{e^{ikR}}{R}\right) \mathrm{d}x_0 \mathrm{d}y_0, \tag{1}$$

and

$$U(x, y, z) = \iint_{\Sigma} [1 - A_0(x_0, y_0)] \frac{\partial}{\partial z}\left(\frac{e^{ikR}}{R}\right) \mathrm{d}x_0 \mathrm{d}y_0, \tag{2}$$

where Σ denotes the clear aperture combining the diffraction mask and its complementary mask, the wavenumber $k = 2\pi/\lambda$, the wavelength is λ, $R^2 = (x - x_0)^2 + (y - y_0)^2 + z^2$, and z is the distance between the mask and the holographic images. In both Eqs. (1) and (2), the incident light is taken as a plane wave with unit amplitude and constant phase. The diffraction pattern of the clear aperture Σ can be taken as $U_\Sigma = U_a + U_b$, where U_Σ is fixed once the aperture Σ is given, and U_a and U_b are variable with high dependence on the spatial distribution of the mask.

Reconstructing two different images by using the complementary masks can be taken as a numerical decomposition of the complex number U_Σ at the image plane. Figure 2(a) sketches the decomposition process in the complex plane, where each complex number is equivalently described as three vectors by following the relationship $U_\Sigma = U_a + U_b$. It offers us a straightforward physical picture of such numerical decomposition. From Fig. 1(a), we can infer that the solution of such decomposition is numerous in mathematics because the intersection point V connecting the vectors U_a and U_b can be located at any position in the entire complex plane. In fact, its desired physical solution in this problem is limited due to the binary target images (which are generated by the diffraction mask and its complementary one, respectively). To illustrate this issue clearly, we exemplify some special cases in Fig. 2(b), which denotes four locations from P_1 to P_4. At the position P_1, the intensity profiles in these two holographic images are zeros, implying that no power is desired at P_1 in both images. However, such requirement $U_a = U_b = 0$ at P_1 is non-physical because the mathematical composition yields a minimum value $U_a = U_b = 0.5U_\Sigma$; see Fig. 2(c). It indicates that the physical solution at P_1 is theoretically non-zero, leaving an undesired background (which is less visible if the contrast of the reconstructed image is high). At the position P_2, both intensity profiles of one can be obtained by taking mathematical solutions, where the intersection point V is located at the perpendicular bisector of the vector U_Σ. Thus, the moduli $|U_a| = |U_b|$ can mathematically take any solution from $0.5|U_\Sigma|$ to ∞. In real cases, the moduli can only be valued

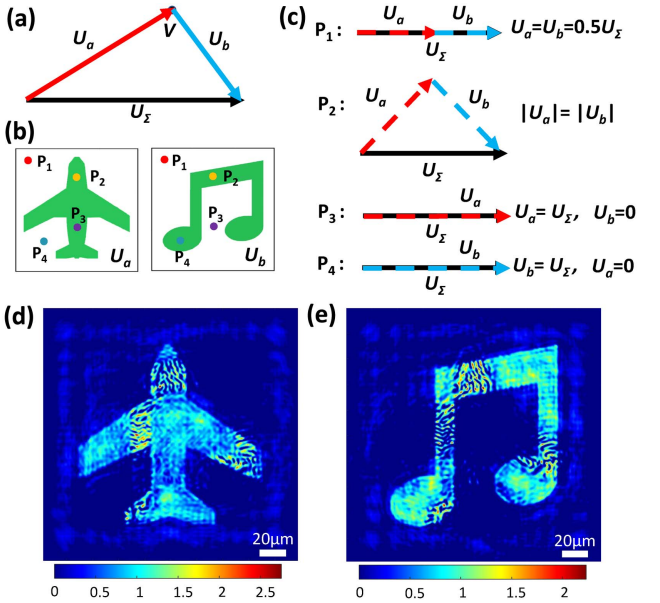

Fig. 2. (a) Numerical decomposition of a complex number U_Σ in terms of a simple summation of two vectors at the complex plane. Each complex number can be expressed equivalently by a vector at the complex plane. Thus, the summation of two complex numbers is visualized by using a summation of two vectors, which helps to understand the hidden mathematics in our proposed physical model. (b) Ideal holographic images with some typical points from P_1 to P_4 that are labelled for better discussion. (c) Physical solutions for different target intensity profiles in both images. (d), (e) Simulated holographic images from (d) the mask and (e) its complementary mask.

within a much smaller range because the energy conservation must be satisfied at the entire image plane, i.e., $\iint(|U_a|^2+|U_b|^2)\mathrm{d}x\mathrm{d}y = \iint|U_\Sigma|^2\mathrm{d}x\mathrm{d}y$. Nevertheless, it is physically possible to create high intensity at P_2, hereby increasing the contrast of the image compared with low intensity at P_1. At the positions P_3 and P_4, the desired electric vectors U_a and U_b at both images are realized physically by making one equal to U_Σ and the other zero; see Fig. 2(c). Through the above discussions, we find that it is feasible in theory to reconstruct two different images by using complementary masks.

To realize this idea, we design two binary-amplitude-type complementary masks using aluminum film sitting on quartz. The squared holes (pixels) etched through the aluminum film are employed as a diffracting aperture for the transmission to produce a holographic pattern, and the rest of the complementary device is responsible for producing another holographic pattern. We start by choosing two target images of an 'airplane' and a 'music note'. The number of pixels of both the target images is 801×801, and each pixel has a pitch of 250 nm × 250 nm, which is smaller than the operating wavelength of 532 nm. Both masks are designed at a propagation distance of 1 mm, which facilitates experimental verification. The design of the device is based on the diffractive surface of aluminum film fabricated on a quartz substrate. One can modify the field pattern on the target plane by manipulating the position and size of the holes for transmitting or reflecting the incoming light. The aluminum film is used here because it is cheaper and absorbs less light in the visible and UV bands than other metals like silver and gold.

A random pixel-by-pixel optimization method is employed to determine the diffraction mask in Fig. 1(a), which is designed to produce the 'airplane' pattern and the complementary mask for the 'music note' pattern. We simulate the optical pattern from each mask by using Rayleigh–Sommerfeld diffraction theory in terms of fast Fourier transform[13,14]. During the optimization process, we systematically simulated all the pixels individually for values '0' and '1' to determine their impact on the target field. The value '1' is for allowing the transmission of light through the diffraction aperture, while '0' represents blocking or reflecting the light using the aluminum film. Each pixel is randomly selected to change its original value to the other one, which leads to the change of both diffraction patterns. The root mean square errors (RMSEs) between the calculated diffraction patterns and their ideal ones are used to evaluate the effectiveness of such change. When the total RMSE as a summation of RMSE_1 for the "airplane" pattern and RMSE_2 for the "music note" pattern is smaller than the original RMSE, such change of value at this selected pixel is taken to be valid and then updated in the mask; otherwise, this change is not accepted. This optimization process is aimed at minimizing the total RMSE. In one round of optimization, all the pixels are selected ergodically, where each pixel is chosen only one time in a single round. This operation allows us to evaluate the weight of every pixel fairly in designing both holographic images. In this work, only four rounds are run at a time cost of ~10 h, which can be shortened further if the parallel computation with a graphics processing unit (GPU) is employed.

Figures 2(d) and 2(e) show the simulated diffraction patterns of the designed mask and its complementary one. It exhibits two different holographic images of the desired "airplane" and "music note," which confirms the feasibility of reconstructing two different images by using complementary masks. As expected, the weak background at the position P_1, where the target intensity values at both images are zero, appears due to the mathematical limitation of the numerical decomposition. Note that the power at each P_1 is smaller than its corresponding total power $|U_\Sigma|^2$ (i.e., $|U_a|^2 + |U_b|^2 < |U_\Sigma|^2$). According to energy conservation, the left power is transferred to other positions (such as P_2 where both images have the same non-zero intensity), which leads to the creation of fringes because of the interference. As expected, in the designed holographic images, we observe the fringes, which are caused by the interference between light at P_2 and the light diffracted from the position P_1. In comparison, the intensity profiles at P_3 and P_4 are highly uniform because the physical solution is possible. More importantly, the intensity profiles at both of the image patterns are much higher than the weak background, thus creating high contrast for a better observation of the image. The device design is relatively simple yet very efficient, easy to fabricate, and can be readily used in industrial applications for holography and imaging.

2.2. Materials

To verify our results experimentally, we transfer the diffraction mask to an AutoCAD file and prepare to fabricate the device. The meta-device is fabricated by depositing a layer of aluminum film on a substrate of quartz (SiO_2). The process of fabricating a device involves coating a positive resist with polymethyl methacrylate (PMMA) at a speed of 3000 r/min, resulting in a thickness of 180 nm on an aluminum film. The coated resist is then exposed to an electron beam to create the desired pattern. The device is developed using a liquid consisting of methyl isobutyl ketone and isopropyl acetone in a 1:3 ratio, which removes the exposed areas, leaving the desired pattern. The exposed areas are then etched away, and the mask is removed, leaving the final device ready for later characterization. The scanning-electron-microscopy (SEM) images are shown in Fig. 3(a), which provides the structural details with different fields of view for a better observation. Due to the complementary features, we exhibit the SEM image of only one sample.

The performance of the aluminum-based mask is evaluated by using the experimental set-up, as shown in Fig. 3(b). We use an illuminating source, which is a supercontinuum laser (SuperK FIANIUM) having a tunable wavelength controlled by an acoustic-optic modulator. The incident beam is modified using a spherical lens and a pinhole followed by another lens for creating a plane wave to illuminate the sample. Since the devices are complementary, we have fabricated two devices, through which we measured the diffraction patterns in the transmission mode. After the transmission, we use an objective to magnify our

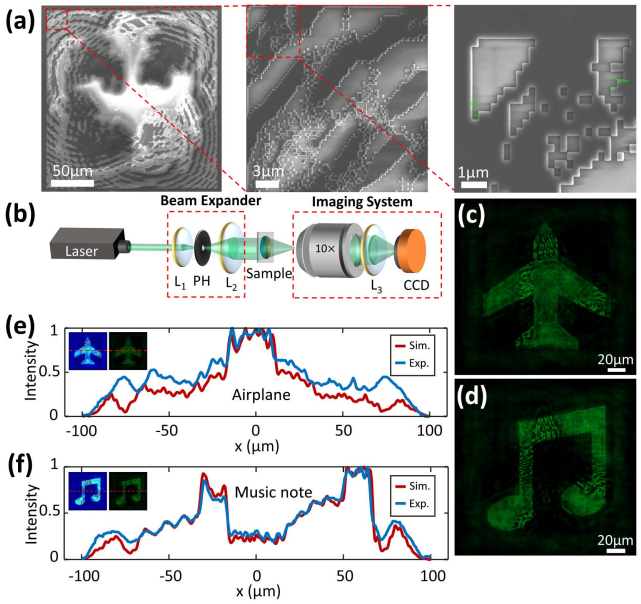

Fig. 3. (a) SEM images of our fabricated mask under different fields of view. (b) Schematic of the experimental setup used to measure the holographic images. L, Lens; PH, pinhole. (c), (d) Measured images of (c) 'airplane' and (d) 'music note' from complementary masks. Scalebars: 20 μm. (e), (f) Simulated (red) and experimental (blue) line scanning intensity profiles of (e) "air plane" and (f) "music note" images. The inserts denote the positions where the line-scanning intensity is selected for both images.

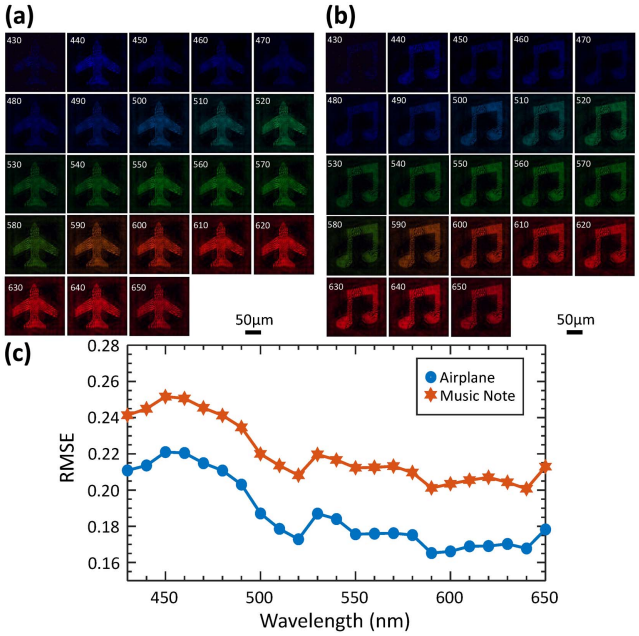

Fig. 4. (a), (b) Measured broadband images "airplane" and "music note" at the wavelengths from 430 nm to 650 nm with a step of 10 nm. (c) Calculated RMSE between the simulated and experimental images for the airplane (blue dots) and the music note (orange stars).

output and a lens to expand the beam to be finally detected by the CCD.

3. Experimental Results

Figures 3(c) and 3(d) show the experimentally measured intensity profiles at the wavelength of 532 nm, exhibiting great consistency with our simulated results. It confirms the validity of our proposed complementary masks for encoding two holographic images. To show the quantitative proofs, a comparison of line scanned intensity is done between the simulated and experimental results, as presented in Figs. 3(e) and 3(f). All of the key features in the holographic images are verified.

Furthermore, we also measure the diffraction efficiency, which is defined as the ratio of the power at the hologram plane to the transmitted intensity at the diffraction plane of the device. A high diffraction efficiency of 88.12% and 91.38% was achieved for the music note and the airplane, respectively. It reveals the efficient light convergence to the target image.

Because the pixel pitch of 250 nm × 250 nm is subwavelength at entire wavelengths, we have also investigated the broadband properties of both complementary masks. Figures 4(a) and 4(b) illustrate the measured intensity profiles for both the holographic images at the wavelength ranging from 450 nm to 650 nm with a step of 10 nm. These holographic images cover blue, green, yellow, and red colors, which make this technique suitable for applications in optical display. From these results, one can observe the clear patterns of the holograms throughout the measurement. To show the image quality, we present their RMSEs, calculated between the simulated and experimental images, in Fig. 4(c). It reveals that the RMSE is less than the 0.25 for all the wavelengths in both holographic images. These values suggest that the differences between the simulated and experimental figures are relatively small, indicating a reasonably good agreement between the two. Thus, we have experimentally verified the broadband capacity of the device, which can be employed as a new technique using complementary structures to produce different images in color-related applications such as display and anti-counterfeiting.

4. Discussions

As Babinet's principle has been successfully applied in metasurfaces as discussed above, it has not been used in holography since complementary surfaces can only be used to block/transmit alternatively and present a similar pattern in both cases (which are usually valid in the Fraunhofer region of aperture-clear complementary masks). However, complementary masks with optimized meta-apertures can be used to produce different results in binary-amplitude optimization, as we have provided in this proposal and experimental verification. Sufficient degrees of freedom provided by the meta-apertures hold for the physical origins of our proposal to realize two different images in their Fresnel regions. It seems a "violation" of Babinet's principle. In fact, our proposed complementary masks that share the same square aperture of finite size are different from those in

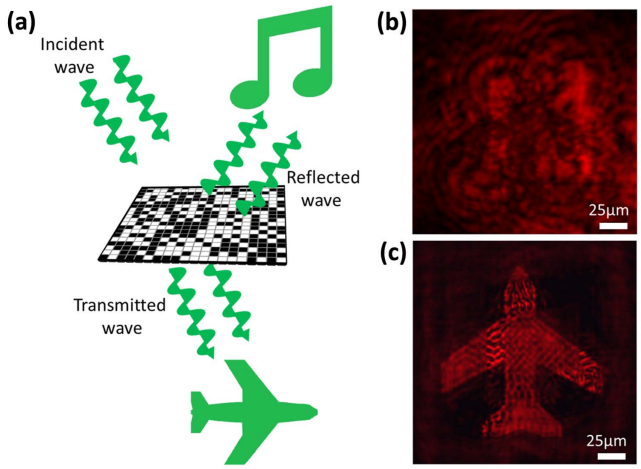

Fig. 5. (a) Schematic of the future application for a light modulating device inspired by Babinet's principle's complementary parts of the diffractive surface. The transmission of a metasurface is meant to produce a pattern of one of the holograms, while the reflection works as a complementary mask to produce another holographic pattern. (b), (c) Measured images in the (b) reflection and (c) transmission sides. Scalebars: 25 μm.

traditional Babinet's principle, where the summation of both complementary masks yields an infinitely large aperture. Rigorously speaking, our proposed complementary masks are not completely equivalent to the complementary masks in Babinet's principle. Therefore, our results cannot be taken as a violation of the traditional Babinet's principle.

To realize the exact Babinet's masks in the transmission mode, one should remove the opaque part outside the shared square aperture in one mask, which needs more complicated fabrication. In fact, the reflected light from one mask is completely complementary to its transmitted light, thus suggesting a rigorous Babinet's mask in a reflective mode. Its potential application is to realize such a device for holography simultaneously in reflection and transmission modes, as sketched in Fig. 5(a). For this purpose, metasurfaces with high reflective efficiency have to be investigated with minimum absorption such that both the transmission and reflection can realize the hologram clearly with minimum noise. Figures 5 (b) and 5(c) illustrate both the reflected and transmitted holographic images, respectively. In the reflected images, the undesired background outside the square aperture of the mask is high so that the useful image is almost undistinguishable. However, the hologram in the reflection mode can be improved in the future by using highly efficient reflective nanostructures on the complementary surface responsible for reflection[6].

5. Conclusion

In conclusion, we have proposed Babinet's principle-inspired metasurfaces to realize two different images from complementary surfaces for holographic display. The hologram has shown a broadband operation of up to 230 nm covering the visible range due to the subwavelength features of the meta-device, with performance matching well with the simulation. Our work provides a general idea and a method to optimize complementary devices to produce different outputs, which might have applications in a variety of fields for modulating different properties of light such as phase, intensity, and polarization.

Acknowledgement

K.H. thanks the National Key Research and Development Program of China (No. 2022YFB3607300), the CAS Project for Young Scientists in Basic Research (No. YSBR-049), the National Natural Science Foundation of China (No. 12134013), the CAS Pioneer Hundred Talents Program, and the University of Science and Technology of China's Centre for Micro and Nanoscale Research and Fabrication for the support. The authors thank Prof. Jinghua Teng for the valuable suggestions and discussions about this work.

References

1. L. Huang, S. Zhang, and T. Zentgraf, "Metasurface holography: from fundamentals to applications," Nanophotonics **7**, 1169 (2018).
2. Y. F. Yu, A. Y. Zhu, R. Paniagua-Domínguez, Y. H. Fu, B. Luk'yanchuk, and A. I. Kuznetsov, "High-transmission dielectric metasurface with 2π phase control at visible wavelengths," Laser Photonics Rev. **9**, 412 (2015).
3. J. Liao, S. Guo, L. Yuan, C. Ji, C. Huang, and X. Luo, "Independent manipulation of reflection amplitude and phase by a single-layer reconfigurable metasurface," Adv. Opt. Mater. **10**, 2101551 (2022).
4. Q. Song, X. Liu, C. W. Qiu, and P. Genevet, "Vectorial metasurface holography," Appl. Phys. Rev. **9**, 011311 (2022).
5. C. Zhang, F. Yue, D. Wen, M. Chen, Z. Zhang, W. Wang, and X. Chen, "Multichannel metasurface for simultaneous control of holograms and twisted light beams," ACS Photonics **4**, 1906 (2017).
6. S. O. H. Mohammed, D. Zhao, S. Y. Azeem, X. Goh, S. J. Tan, J. Teng, and K. Huang, "Efficiency-enhanced reflective nanosieve holograms," Chin. Opt. Lett. **20**, 053602 (2022).
7. B. Wang, B. Quan, J. He, Z. Xie, X. Wang, J. Li, and Y. Zhang, "Wavelength de-multiplexing metasurface hologram," Sci. Rep. **6**, 35657 (2016).
8. Z. L. Deng and G. Li, "Metasurface optical holography," Mater. Today Phys. **3**, 51 (2017).
9. C. F. Bohren and D. R. Huffman, *Absorption and Scattering of Light by Small Particles* (Wiley, 2004).
10. F. Falcone, T. Lopetegi, M. A. G. Laso, J. D. Baena, J. Bonache, M. Beruete, R. Marqués, F. Martín, and M. Sorolla, "Babinet principle applied to the design of metasurfaces and metamaterials," Phys. Rev. Lett. **93**, 197401 (2004).
11. X. Luo, F. Hu, and G. Li, "Dynamically reversible and strong circular dichroism based on Babinet-invertible chiral metasurfaces," Opt. Lett. **46**, 1309 (2021).
12. Y. Nakata, Y. Urade, K. Okimura, T. Nakanishi, F. Miyamaru, M. W. Takeda, and M. Kitano, "Anisotropic Babinet-invertible metasurfaces to realize transmission-reflection switching for orthogonal polarizations of light," Phys. Rev. Appl. **6**, 044022 (2016).
13. F. Shen and A. Wang, "Fast-Fourier-transform based numerical integration method for the Rayleigh–Sommerfeld diffraction formula," Appl. Opt. **45**, 1102 (2006).
14. K. Huang, F. Qin, H. Liu, H. Ye, C. Qiu, M. Hong, B. Luk'yanchuk, and J. Teng, "Planar diffractive lenses: fundamentals, functionalities, and applications," Adv. Mater. **30**, 1704556 (2018).